PROCEEDINGS A

rspa.royalsocietypublishing.org

Research

Cite this article: Dey S, Ali SZ. 2017 Origin of the onset of meandering of a straight river. *Proc. R. Soc. A* **473**: 20170376.
http://dx.doi.org/10.1098/rspa.2017.0376

Received: 29 May 2017
Accepted: 17 July 2017

Subject Areas:
geophysics, fluid mechanics

Keywords:
river meandering, turbulent flow, sediment transport

Authors for correspondence:
Subhasish Dey
e-mail: sdey@iitkgp.ac.in
Sk Zeeshan Ali
e-mail: skzeeshanali@iitkgp.ac.in

Origin of the onset of meandering of a straight river

Subhasish Dey[1,2,3] and Sk Zeeshan Ali[1]

[1]Department of Civil Engineering, Indian Institute of Technology Kharagpur, West Bengal 721302, India
[2]Physics and Applied Mathematics Unit, Indian Statistical Institute, Kolkata, West Bengal 700108, India
[3]Department of Hydraulic Engineering, State Key Laboratory of Hydro-Science and Engineering, Tsinghua University, Beijing 100084, People's Republic of China

SZA, 0000-0003-0763-7437

In this paper, to explore the origin of the onset of meandering of a straight river, we, first, analyse the linear stability of a straight river. We discover that the natural perturbation modes of a straight river maintain an equilibrium state by confining themselves to an onset wavenumber band that is dependent on the flow regimes, aspect ratio, relative roughness number and Shields number. Then, we put forward a phenomenological description of the onset of meandering of a straight river. Its mechanism is governed by turbulent flow, with counter-rotation of neighbouring large-scale or macro-turbulent eddies in succession to generate the processes of alternating erosion and deposition of sediment grains of the riverbed. This concept is explained by a theorem (universal scaling law) stemming from the phenomenology of a turbulent energy cascade to provide a quantitative insight into the criterion for the onset of meandering of a straight river. It is revealed from this universal scaling law that, at the onset of meandering of a river, the longitudinal riverbed slope is a unique function of the river width, flow discharge and sediment grain size. This unique functional relationship is corroborated by the data obtained from the measurements in natural and model rivers.

1. Introduction

The twists and turns of a natural river flow in a developed meandering course are ubiquitous and enchanting features of planetary surfaces [1–3]. Meandering patterns are strongly associated with

THE ROYAL SOCIETY PUBLISHING

environmental and anthropogenic influences. They also have many implications in flood control, riverbank stabilization, agricultural land preservation and many others [4]. Numerous studies were reported to understand the principal mechanism [5], in conjunction with the topology [6,7] and the maintenance [8], of the meandering of a river. The revolution of the Earth [9,10], riverbed instability [11,12], helicoidal flow [13,14], excess flow energy [15] and macro-turbulent eddies [16] are the existing concepts associated with the formation of a meandering course of rivers. Why and when does a straight river meander? In the *Codex Arundel*, Leonardo da Vinci (1452–1519) portrayed the migration of meanders of a riverbed in the form of a wave in the downstream direction. Such an image of a gravity wave was later established through measurements [17]. Although several conceptual mechanisms were reported in the past to provide plausible explanations for this [5,18], the true onset of meandering of a straight river remains a puzzling phenomenon.

A rather simple onset criterion for a river to meander was stated by linking the critical longitudinal riverbed slope S and the flow discharge Q. This criterion tells us that, at the onset, $S = aQ^b$, where a and b are empirical constants [19]. Analysing the data from numerous natural and model rivers, the empirical constants were found to be $a = 7 \times 10^{-4}\ \mathrm{m^{3/4}\,s^{-1/4}}$ and $b = -0.25$. This simplified functional relationship implies that, when the flow discharge in a river increases, a lesser riverbed slope leads to the establishment of a true meandering course of a river. Later, an attempt was made to introduce the effects of the sediment grain size to the onset criterion [12]. However, these relationships, solely based on the empirical foundation, are dimensionally inhomogeneous and thus invite uncertainties. The concept of the sine-generated curve was also introduced to find the most likely path between static points [20]. It was shown that a criterion for the most likely path of a continuous curve can be found if the global curvature attains a minimum value. The underlying assumption of this concept was that, for a specific number of steps, the changeover of the direction at the extremity of each step follows a normal distribution. Then, following the principle of minimum variance, it was stated that a meandering river is more stable than a straight river [21]. Mecklenburg & Jayakaran [22] obtained the salient dimensions of a meandering river by performing the integrals of the sine and cosine of the sine-generated curve. Moreover, a detailed stochastic description of the meandering of a river was put forward by Movshovitz-Hadar & Shmukler [23].

In 1977, Yalin [16] stated that the onset of the meandering of a river was governed by large-scale or macro-turbulent eddies. It was argued that the macro-turbulent eddies possess a longitudinal length scale roughly equalling the longitudinal length of alternate bars in a straight river. The length scale of the macro-turbulent eddies was surmised to be six times the river width. Such a consideration of the alternate bar formation at approximately regular intervals was equivalent to that of dune formation initiated by these eddies. This concept can only provide a qualitative idea of the meandering of a river; however, an acceptable fundamental mechanism and a quantification of the onset criterion of the meandering of a straight river remain unknown.

So far, the stability analysis of the formation of alternate bars in a straight river has been proved to be a successful tool to assess the onset of the meandering of a river [24–27]. Such an analysis can anticipate whether a straight river would maintain a straight course, form alternate bars or become a braided river. However, with regard to the stability analysis, the fundamental question is whether there is any specific band of wavenumbers which govern the onset of the meandering of a river over a wide range of physical variables? Moreover, how does this band of wavenumbers respond to external perturbations? Furthermore, is the extent of this band dependent on the flow regimes? Given these questions, the main objective of this study is to address these important issues and to establish a viable theoretical description of the background mechanism that leads to the origin of the onset of the meandering of a straight river from the phenomenology of a turbulent energy cascade [28].

The paper is organized as follows. In §2, a stability analysis of a straight river is performed. The phenomenological framework of the onset of the meandering of a straight river is described in §3. Finally, the conclusion is drawn in §4.

2. Stability analysis

(a) Mathematical formulation

Let us consider a straight unperturbed river confined to two parallel guided boundaries flowing over an erodible sediment bed (figure 1). The river has a constant width of $2\mathcal{B}$ (figure 1*a* and table 1). We choose a Cartesian coordinate system (x, y), where x represents the longitudinal distance and y denotes the spanwise distance measured from the river centreline. The depth-averaged velocity components in (x, y) are given by $(\mathcal{U}, \mathcal{V})$, respectively. The $\mathcal{D}$ and $\mathcal{H}$ are the local flow depth and the height of the free surface from a fixed reference level, respectively (figure 1*b*,*c*), and z denotes the vertical distance measured from a fixed reference level (figure 1*c*). Let the components of the bed shear stress and the volumetric sediment flux in (x, y) be (T_x, T_y) and (Q_x, Q_y), respectively.

To perform a stability analysis, the equations of motion can be derived by performing a depth-averaging of the time-averaged momentum equations of flow together with the suitable boundary conditions, including the time-averaged pressure intensity to obey the hydrostatic law. It is however relevant to mention that the effects of secondary currents are not included in the stability analysis, although we admit that these effects can be important in the case of a narrow river flow. In addition, the considerations of the depth-averaged continuity equation of flow and the continuity equation of sediment flux are pertinent to accomplish the stability analysis.

The momentum equations of flow are [29]

$$\hat{\mathcal{U}}\frac{\partial\hat{\mathcal{U}}}{\partial\hat{x}}+\hat{\mathcal{V}}\frac{\partial\hat{\mathcal{U}}}{\partial\hat{y}}+\frac{\partial\hat{\mathcal{H}}}{\partial\hat{x}}+\mathcal{A}\frac{\hat{T}_x}{\hat{\mathcal{D}}}=0 \tag{2.1}$$

and

$$\hat{\mathcal{U}}\frac{\partial\hat{\mathcal{V}}}{\partial\hat{x}}+\hat{\mathcal{V}}\frac{\partial\hat{\mathcal{V}}}{\partial\hat{y}}+\frac{\partial\hat{\mathcal{H}}}{\partial\hat{y}}+\mathcal{A}\frac{\hat{T}_y}{\hat{\mathcal{D}}}=0. \tag{2.2}$$

The continuity equation of flow is [29]

$$\frac{\partial}{\partial\hat{x}}(\hat{\mathcal{D}}\hat{\mathcal{U}})+\frac{\partial}{\partial\hat{y}}(\hat{\mathcal{D}}\hat{\mathcal{V}})=0. \tag{2.3}$$

On the other hand, the continuity equation of sediment flux is [30]

$$\frac{\partial}{\partial\hat{t}}(\mathcal{F}^2\hat{\mathcal{H}}-\hat{\mathcal{D}})+\frac{\partial\Phi_x}{\partial\hat{x}}+\frac{\partial\Phi_y}{\partial\hat{y}}=0. \tag{2.4}$$

In equations (2.1)–(2.4), the following non-dimensional variables are introduced:

$$\left.\begin{aligned}&(\hat{x},\hat{y})=\frac{(x,y)}{\mathcal{B}},\quad \hat{\mathcal{D}}=\frac{\mathcal{D}}{\mathcal{D}_m},\quad \hat{\mathcal{H}}=\frac{\mathcal{H}}{\mathcal{F}^2\mathcal{D}_m},\quad \mathcal{F}=\frac{\mathcal{U}_m}{(g\mathcal{D}_m)^{1/2}},\quad \mathcal{A}=\frac{\mathcal{B}}{\mathcal{D}_m},\\&(\hat{\mathcal{U}},\hat{\mathcal{V}})=\frac{(\mathcal{U},\mathcal{V})}{\mathcal{U}_m},\quad (\hat{T}_x,\hat{T}_y)=\frac{(T_x,T_y)}{\rho_f\mathcal{U}_m^2}\\&\text{and}\qquad \hat{t}=t\frac{\mathcal{U}_m Q_r}{\mathcal{B}},\quad Q_r=\frac{(\Delta g d^3)^{1/2}}{(1-\rho_0)\mathcal{U}_m\mathcal{D}_m},\quad (\Phi_x,\Phi_y)=\frac{(Q_x,Q_y)}{(\Delta g d^3)^{1/2}},\end{aligned}\right\} \tag{2.5}$$

where subscript m (also in the subsequent sections) denotes the quantities associated with the unperturbed uniform flow, $\mathcal{F}$ is the unperturbed flow Froude number, g is the gravitational acceleration, $\mathcal{A}$ is the aspect ratio, ρ_f is the mass density of fluid, t is the time, Q_r is the ratio of the characteristic scale of sediment flux to flow flux, Δ is the submerged relative density of the sediment grains $[=(\rho_p-\rho_f)/\rho_f]$, ρ_p is the mass density of the sediment grains, ρ_0 is the porosity of the sediment and d is the median size of the sediment grains.

In essence, the physical condition suggests that the guided boundaries are impermeable both to the fluid flux and to the sediment flux. It is worth mentioning that these boundary conditions are valid even for the erodible guided boundaries, where it can be assumed that the bank erosion

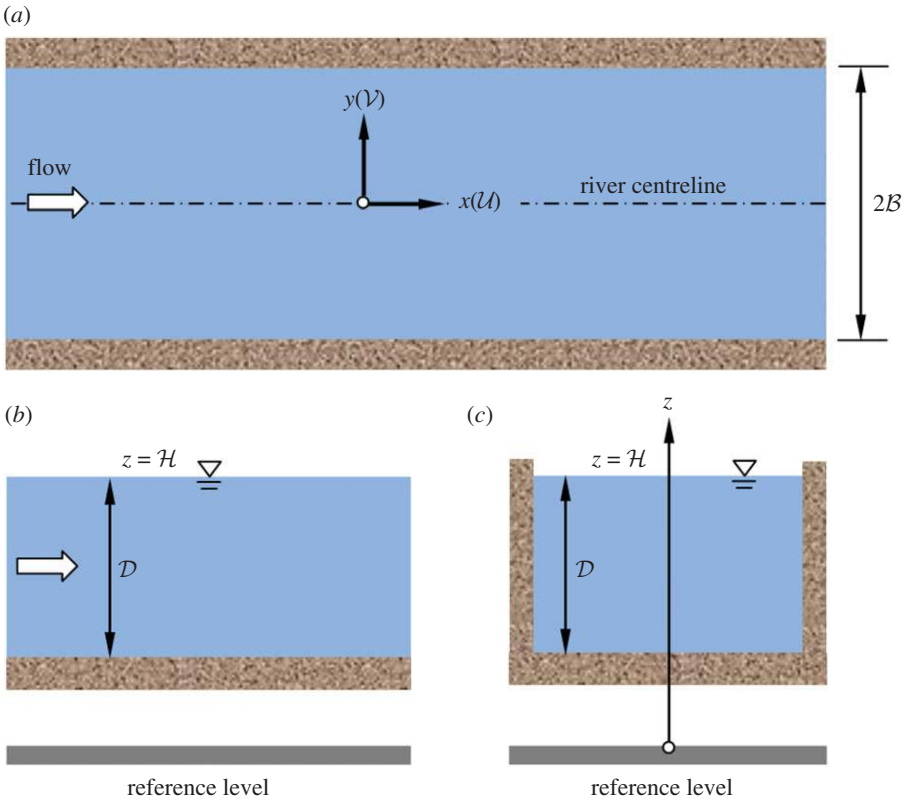

Figure 1. Schematic of a straight unperturbed river: (*a*) plan view, (*b*) longitudinal view and (*c*) cross-sectional view. (Online version in colour.)

rate is so slow that the flow field is hardly affected. Thus, in implicit form, it can be assumed that a slowly moving boundary can be considered to be a fixed boundary at lowest order. Hence, the boundary conditions accompanying equations (2.1)–(2.4) are $\hat{\mathcal{V}}(\hat{y}=\pm 1)=\Phi_y(\hat{y}=\pm 1)=0$.

The components of the bed shear stress $(\hat{T}_x, \hat{T}_y)$ are expressed as

$$(\hat{T}_x, \hat{T}_y)=\frac{f}{8}(\hat{\mathcal{U}}, \hat{\mathcal{V}})(\hat{\mathcal{U}}^2+\hat{\mathcal{V}}^2)^{1/2}, \tag{2.6}$$

where f is the Darcy–Weisbach friction factor. The f can be determined from the well-known Colebrook–White equation [31]. It is given by

$$\frac{1}{f^{1/2}}=\frac{1}{8^{1/2}}\frac{\mathcal{U}}{u_*}=-0.86\ln\left[\left(\frac{\hat{k}_s}{14.8\hat{\mathcal{D}}}\right)^{1.1}+\frac{2.51}{\mathcal{R}f^{1/2}}\right], \tag{2.7}$$

where u_* is the friction velocity, $\hat{k}_s$ is $k_s/\mathcal{D}_m$, k_s is the bed roughness height, $\mathcal{R}$ is the flow Reynolds number $(=4\mathcal{U}\mathcal{D}/\nu)$ and ν is the coefficient of kinematic viscosity of the fluid. The k_s can be expressed as $k_s=\alpha d$, where α is a multiplicative constant. From experimental observation, we set $\alpha=2.5$ [32]. The primary advantage of using the Colebrook–White equation is that it provides an estimation of the friction factor covering a broad spectrum of flow regimes (hydraulically smooth, transitional and rough flow regimes). Importantly, in a hydraulically rough flow regime, a different relationship, for instance Einstein's [33] friction factor formula, could be used because the Colebrook–White equation closely corresponds to Einstein's [33] formula. However, in hydraulically transitional and rough flow regimes, Einstein's [33] formula cannot be applicable.

Table 1. Nomenclature.

$\mathcal{A}$	aspect ratio ($=\mathcal{B}/\mathcal{D}_m$)
$\mathcal{B}$	river half-width
$\mathcal{D}$	local flow depth
$\hat{\mathcal{D}}$	$\mathcal{D}/\mathcal{D}_m$
d	median size of sediment grains
$E(k_w)$	turbulent energy spectrum function
E_1, E_2	macro-turbulent eddies
e_1	micro-turbulent eddies
$\mathcal{F}$	unperturbed flow Froude number ($=\mathcal{U}_m/(g\mathcal{D}_m)^{1/2}$)
f	Darcy–Weisbach friction factor
$\mathcal{G}$	Galileo number ($=\Delta g d^3/\nu^2$)
g	gravitational acceleration
$\mathcal{H}$	height of the free surface from a fixed reference level
$\hat{\mathcal{H}}$	$\mathcal{H}/\mathcal{F}^2\mathcal{D}_m$
i	imaginary unit satisfying $i^2=-1$
$i\omega$	complex quantity
k_s	bed roughness height
k_w	eddy wavenumber
$\hat{k}$	non-dimensional meander wavenumber
$\hat{k}_s$	$k_s/\mathcal{D}_m$
L	length scale of macro-turbulent eddies
L_{mw}	meandering wavelength
l	length scale of micro-turbulent eddies
M	$0.5(2m+1)\pi$
m	natural integer
Q	flow discharge
Q_r	$(\Delta g d^3)^{1/2}/[(1-\rho_0)\mathcal{U}_m\mathcal{D}_m]$
Q_x, Q_y	components of volumetric sediment flux in (x, y)
$\mathcal{R}$	flow Reynolds number ($=4\mathcal{U}\mathcal{D}/\nu$)
$\mathcal{R}_*$	shear Reynolds number ($=u_* k_s/\nu$)
S	longitudinal riverbed slope
T_x, T_y	components of bed shear stress in (x, y)
$\hat{T}_x, \hat{T}_y$	$(T_x, T_y)/\rho_f\mathcal{U}_m^2$
t	time
$\hat{t}$	$t\mathcal{U}_m Q_r/\mathcal{B}$
$(\mathcal{U}, \mathcal{V})$	depth-averaged velocity components in (x, y)
U_L	velocity scale of macro-turbulent eddies
$\mathcal{U}_w$	speed of gravity waves

(*Continued.*)

Table 1. (*Continued*.)

$(\hat{\mathcal{U}}, \hat{\mathcal{V}})$	$(\mathcal{U}, \mathcal{V})/\mathcal{U}_m$
u_l	velocity scale of micro-turbulent eddies
u_n	normal velocity component of u_l
u_t	tangential velocity component of u_l
u_*	friction velocity
(x, y, z)	Cartesian coordinate system
$(\hat{x}, \hat{y})$	$(x, y)/\mathcal{B}$
Δ	submerged relative density of sediment grains $(= (\rho_\mathrm{p} - \rho_\mathrm{f})/\rho_\mathrm{f})$
(Φ_x, Φ_y)	$(Q_x, Q_y)/(\Delta g d^3)^{1/2}$
Θ	Shields number $(= u_*^2/(\Delta g d))$
Θ_c	Shields number at onset of a grain motion
α	k_s/d
β	angle subtended by the trajectory of a sediment grain with the longitudinal direction
δ	angle between the local shear stress vector and the longitudinal direction
ν	coefficient of kinematic viscosity of fluid
ρ_f	mass density of fluid
ρ_p	mass density of sediment grains
ρ_0	porosity of sediment
σ	spectral exponent
τ_f	fluid shear stress at the riverbed
τ_g	gravitational stress generated at the riverbed
ζ	relative roughness number $(= d/\mathcal{D}_m)$
subscript 'm'	quantities associated with unperturbed uniform flow

Thus, in hydraulically transitional and rough flow regimes, the model results would be affected if a different friction factor formula were employed instead of using the Colebrook–White equation.

We recall two crucial parameters, namely the shear Reynolds number $\mathcal{R}_*$, which signifies the relative contribution of fluid inertia to viscous damping, and the Shields number Θ, which indicates the non-dimensional fluid-induced bed shear stress. They are defined as [18]

$$\mathcal{R}_* = \frac{u_* k_\mathrm{s}}{\nu} \quad \text{and} \quad \Theta = \frac{u_*^2}{\Delta g d}. \tag{2.8}$$

The $\mathcal{R}_*$ and Θ can be coupled as $\mathcal{R}_* = \alpha(\mathcal{G}\Theta)^{1/2}$, where $\mathcal{G}$ is the Galileo number $(= \Delta g d^3/\nu^2)$. Thus, the Froude number $\mathcal{F}$ and the Reynolds number $\mathcal{R}$ can be rewritten as $\mathcal{F} = (8\Delta\zeta\Theta/f)^{1/2}$ and $\mathcal{R} = 4\hat{\mathcal{D}}\mathcal{R}_*(\alpha\zeta)^{-1}(8/f)^{1/2}$, where ζ is the relative roughness number $(= d/\mathcal{D}_m)$.

The components of the volumetric sediment flux (Φ_x, Φ_y) are expressed as $(\Phi_x, \Phi_y) = \Phi(\cos\beta, \sin\beta)$, where β is the angle subtended by the trajectory of the sediment grain with the longitudinal direction. It is given by [34]

$$\beta = \sin^{-1}\left[\sin\delta - \frac{r}{\mathcal{A}\Theta^{1/2}}\frac{\partial}{\partial\hat{y}}(\mathcal{F}^2\hat{\mathcal{H}} - \hat{\mathcal{D}})\right], \tag{2.9}$$

where δ is the angle between the local shear stress vector and the longitudinal direction and r is a coefficient approximately equalling 0.5 [35]. The δ is expressed as $\delta = \sin^{-1}[\hat{\mathcal{V}}/(\hat{\mathcal{U}}^2 + \hat{\mathcal{V}}^2)^{1/2}]$.

The dominant mode of sediment transport in this study is considered to be the bedload transport. Therefore, the Φ can be obtained from the Meyer–Peter–Müller formula [18], which is given by

$$\Phi = 8(\Theta - \Theta_c)^{3/2}, \tag{2.10}$$

where Θ_c is the Shields number at the onset of grain motion. It may be noted that the Meyer–Peter–Müller formula corresponds well with the experimental data for coarse sands and gravels. Furthermore, the interesting feature of the Meyer–Peter–Müller formula is that it expresses Φ in the form of a power function, which ensures a smooth trend of the derivative $\partial\Phi/\partial\Theta$ without hampering the continuity. The other well-established empirical relationships for Φ do not have such a flexibility. Hence, the model results would invite discontinuities in the evolution of the growth rate of external perturbation if an empirical relationship other than the Meyer–Peter–Müller formula were used. The determination of Θ_c (see equation (2.10)) requires an in-depth analysis of the motivating hydrodynamic forces that act on the sediment grains in conjunction with the near-bed turbulence effects [36]. However, to simplify the analysis, the Θ_c can be determined from the following set of empirical relationships [37]:

$$\left.\begin{aligned} &\Theta_c(\mathcal{G} \le 43.7) = 0.141\mathcal{G}^{-0.115}, \\ &\Theta_c(43.7 < \mathcal{G} < 79998.5) = \frac{[1 + (0.022\sqrt{\mathcal{G}})^{2.84}]^{0.35}}{3.09\mathcal{G}^{0.34}} \\ \text{and}\quad &\Theta_c(\mathcal{G} \ge 79998.5) = 0.045. \end{aligned}\right\} \tag{2.11}$$

We now perform a normal-mode analysis of the primitive variables $(\hat{\mathcal{U}}, \hat{\mathcal{V}}, \hat{\mathcal{H}}, \hat{\mathcal{D}})$ by setting the following regular expansions:

$$(\hat{\mathcal{U}}, \hat{\mathcal{V}}, \hat{\mathcal{H}}, \hat{\mathcal{D}}) = (1, 0, \hat{\mathcal{H}}_m, 1) + \varepsilon[(\tilde{\mathcal{U}}, \tilde{\mathcal{V}}, \tilde{\mathcal{H}}, \tilde{\mathcal{D}}) \exp \mathrm{i}(\hat{k}\hat{x} - \omega\hat{t}) + \text{c.c.}] + \mathcal{O}(\varepsilon^2), \tag{2.12}$$

where ε is $\mathcal{O}(1)$, i is the imaginary unit satisfying $\mathrm{i}^2 = -1$, $\hat{k}$ is the non-dimensional wavenumber, $-\mathrm{i}\omega$ is the complex quantity, whose real and imaginary parts signify the growth rate and the non-dimensional frequency, respectively, and c.c. represents the complex conjugate.

Applying equation (2.12), the Taylor series expansions of the $\hat{T}_x$ and the Φ yield

$$\hat{T}_x = \frac{f_m}{8}\{1 + \varepsilon[(\tilde{\mathcal{U}}c_1 + \tilde{\mathcal{D}}c_2) \exp \mathrm{i}(\hat{k}\hat{x} - \omega\hat{t}) + \text{c.c. }]\} + \mathcal{O}(\varepsilon^2) \tag{2.13}$$

and

$$\Phi = \Phi_m\{1 + \varepsilon[(\tilde{\mathcal{U}}c_3 + \tilde{\mathcal{D}}c_4) \exp \mathrm{i}(\hat{k}\hat{x} - \omega\hat{t}) + \text{c.c.}]\} + \mathcal{O}(\varepsilon^2), \tag{2.14}$$

where

$$\left.\begin{aligned} &c_1 = 2\left(1 - \frac{\Theta_m}{f_m}\frac{\partial f}{\partial \Theta}\right)^{-1}, \quad c_2 = \frac{1}{f_m}\frac{\partial f}{\partial \hat{\mathcal{D}}}\left(1 - \frac{\Theta_m}{f_m}\frac{\partial f}{\partial \Theta}\right)^{-1} \\ \text{and}\quad &c_3 = \frac{\Theta_m}{\Phi_m}\frac{\partial \Phi}{\partial \Theta}c_1, c_4 = \frac{\Theta_m}{\Phi_m}\frac{\partial \Phi}{\partial \Theta}c_2 + \frac{1}{\Phi_m}\frac{\partial \Phi}{\partial \hat{\mathcal{D}}}. \end{aligned}\right\} \tag{2.15}$$

Substituting equation (2.12) into the governing equations (2.1)–(2.4) and using equations (2.13) and (2.14), we obtain the following set of equations at $\mathcal{O}(\varepsilon)$ in matrix form:

$$\begin{pmatrix} a_{11} & a_{12} & a_{13} & a_{14} \\ a_{21} & a_{22} & a_{23}\dfrac{\mathrm{d}}{\mathrm{d}\hat{y}} & a_{24} \\ a_{31} & a_{32}\dfrac{\mathrm{d}}{\mathrm{d}\hat{y}} & a_{33} & a_{34} \\ a_{41} & a_{42}\dfrac{\mathrm{d}}{\mathrm{d}\hat{y}} & a_{43}\dfrac{\mathrm{d}^2}{\mathrm{d}\hat{y}^2} & a_{44}\dfrac{\mathrm{d}^2}{\mathrm{d}\hat{y}^2} + a_{45} \end{pmatrix} \begin{pmatrix} \tilde{\mathcal{U}} \\ \tilde{\mathcal{V}} \\ \tilde{\mathcal{H}} \\ \tilde{\mathcal{D}} \end{pmatrix} = \begin{pmatrix} b_1 \\ b_2 \\ b_3 \\ b_4 \end{pmatrix}, \tag{2.16}$$

where the matrix coefficients are given by

$$\left.\begin{aligned} &a_{11}=\Psi c_1+\mathrm{i}\hat{k},\quad a_{12}=a_{21}=a_{24}=a_{33}=b_1=b_2=b_3=0,\quad a_{13}=a_{31}=a_{34}=\mathrm{i}\hat{k},\\ &a_{14}=\Psi(c_2-1),\quad a_{22}=\Psi+\mathrm{i}\hat{k},\quad a_{23}=a_{32}=a_{42}=1,\quad a_{41}=\mathrm{i}\hat{k}c_3,\quad a_{43}=-\frac{r}{\mathcal{A}\Theta^{1/2}}\mathcal{F}^2\\ \text{and}\quad &a_{44}=\frac{r}{\mathcal{A}\Theta^{1/2}},\quad a_{45}=\mathrm{i}\hat{k}c_4,\quad b_4=\frac{\mathrm{i}\omega(\mathcal{F}^2\tilde{\mathcal{H}}-\tilde{\mathcal{D}})}{\Phi_m},\quad \Psi=\mathcal{A}\frac{f_m}{8}. \end{aligned}\right\} \tag{2.17}$$

The boundary conditions allow us to seek the solutions as follows: $(\tilde{\mathcal{U}},\tilde{\mathcal{H}},\tilde{\mathcal{D}})=(\tilde{\mathcal{U}}_0,\tilde{\mathcal{H}}_0,\tilde{\mathcal{D}}_0)\sin M\hat{y}$ and $\tilde{\mathcal{V}}=\tilde{\mathcal{V}}_0\cos M\hat{y}$, where $M=0.5(2m+1)\pi$ and m is a natural integer that predicts the river pattern. To be explicit, $m=0$ indicates the onset of the formation of alternate bars (as considered here), whereas $m>1$ signifies the affinity of a river to braid. Substituting the forms of $\tilde{\mathcal{U}}$, $\tilde{\mathcal{V}}$, $\tilde{\mathcal{H}}$ and $\tilde{\mathcal{D}}$ into the relationship (2.16) and after rearrangement, the complex quantity $-\mathrm{i}\omega$ is obtained as follows:

$$\begin{aligned} &\frac{-\mathrm{i}\omega\{\mathcal{F}^2[(a_{11}-a_{14})a_{22}a_{31}]-[a_{13}a_{22}a_{31}-a_{11}M^2]\}}{\Phi_m}\\ &\quad=(a_{13}a_{22}a_{31}-a_{11}M^2)\left[a_{44}M^2-a_{45}+\frac{a_{14}a_{41}}{a_{11}}\right]\\ &\qquad+(a_{11}-a_{14})a_{22}a_{31}\left[\left(a_{43}-\frac{1}{a_{22}}\right)M^2+\frac{a_{13}a_{41}}{a_{11}}\right]. \end{aligned} \tag{2.18}$$

(b) Results and discussion

From the theoretical analysis, it is obvious that the real and the imaginary parts of $-\mathrm{i}\omega$, $\mathrm{Re}(-\mathrm{i}\omega)$ and $\mathrm{Im}(-\mathrm{i}\omega)$, respectively, are the functions of the aspect ratio $\mathcal{A}$, the relative roughness number ζ and the Shields number Θ. Thus, as a functional representation, we can write $[\mathrm{Re}(-\mathrm{i}\omega),\ \mathrm{Im}(-\mathrm{i}\omega)]=F(\mathcal{A},\zeta,\Theta)$, where the function F typically depends on different flow regimes by means of the friction factor conjecture (equation (2.7)). To cover the entire flow regimes, we consider the shear Reynolds number $\mathcal{R}_*=4$, 20 and 500, corresponding to the hydraulically smooth, transitional and rough flow regimes, respectively. Furthermore, the mass densities of the fluid and sediment grains are considered as $\rho_\mathrm{f}=10^3\,\mathrm{kg\,m^{-3}}$ and $\rho_\mathrm{p}=2.65\times10^3\,\mathrm{kg\,m^{-3}}$, respectively. Specifically, the condition $\mathrm{Re}(-\mathrm{i}\omega)>0$ suggests an exponential growth rate, whereas the condition $\mathrm{Re}(-\mathrm{i}\omega)<0$ signifies an exponential decay rate. Figure 2*a–c* depicts the variations of $\mathrm{Re}(-\mathrm{i}\omega)$ and $\mathrm{Im}(-\mathrm{i}\omega)$ with non-dimensional wavenumber $\hat{k}$ for $\mathcal{A}=30$, $\zeta=0.005$, $\Theta=0.2$, 0.4, 0.6 and 0.8, and $\mathcal{R}_*=4$, 20 and 500. For a specific $\mathcal{R}_*$ and Θ, a quick response of the straight river to the external perturbations is notable, because the variations of $\mathrm{Re}(-\mathrm{i}\omega)$ with $\hat{k}$ show an exponential growth or decay, except in the neighbourhood of $\hat{k}\approx0.1$. This indicates the inherent instability of a straight river subjected to erosion and deposition of sediment grains aided by the external variables. For a given $\hat{k}$ with $\hat{k}\ll0.1$, the $\mathrm{Re}(-\mathrm{i}\omega)$ decays with an increase in Θ (figure 2*a–c*). By contrast, for a given $\hat{k}$ with $\hat{k}>0.1$, the $\mathrm{Re}(-\mathrm{i}\omega)$ increases with Θ. However, this is not the case when $\hat{k}$ approaches unity. For a given $\hat{k}$ with $\hat{k}\approx1$, the $\mathrm{Re}(-\mathrm{i}\omega)$ for a larger Θ (= 0.4, 0.6 and 0.8) grows abruptly with a high frequency. The variations of $\mathrm{Im}(-\mathrm{i}\omega)$ with $\hat{k}$ for a specific flow regime suggest that, for a given $\hat{k}$ with $\hat{k}\ll0.1$, the frequency of excitation is almost invariant of Θ. However, for a given $\hat{k}$ with $\hat{k}>0.1$, the frequency of excitation sharply increases with Θ (figure 2*a–c*).

We now turn our attention to a small window of wavenumbers $\hat{k}\in[0.05,0.15]$, where both the values of $\mathrm{Re}(-\mathrm{i}\omega)$ and $\mathrm{Im}(-\mathrm{i}\omega)$ are marginally small, say $[\mathrm{Re}(-\mathrm{i}\omega),\ \mathrm{Im}(-\mathrm{i}\omega)]\in[-0.05,0.05]$, as shown in the insets of figure 2*a–c*. Interestingly, for a specific flow regime, there exists a band of wavenumbers $\hat{k}_c$ featured by $\{\hat{k}_c:[\mathrm{Re}(-\mathrm{i}\omega),\mathrm{Im}(-\mathrm{i}\omega)]\in[-0.05,0.05]\forall\Theta\in[0.2,0.8]\}$. In a generalized form, using the notations of set theory, we can write $\hat{k}_c=\hat{k}\{[\mathrm{Re}(-\mathrm{i}\omega),\ \mathrm{Im}(-\mathrm{i}\omega)](\Theta=\Theta_1)\}\cap\hat{k}\{[\mathrm{Re}(-\mathrm{i}\omega),\ \mathrm{Im}(-\mathrm{i}\omega)](\Theta=\Theta_2)\}\ldots$ subject to the conditions: $[\mathrm{Re}(-\mathrm{i}\omega),\ \mathrm{Im}(-\mathrm{i}\omega)]\in[-0.05,0.05]$ and $(\Theta_1,\Theta_2,\ldots)\in[\Theta_\mathrm{l},\Theta_\mathrm{u}]$, where subscripts 'l' and 'u'

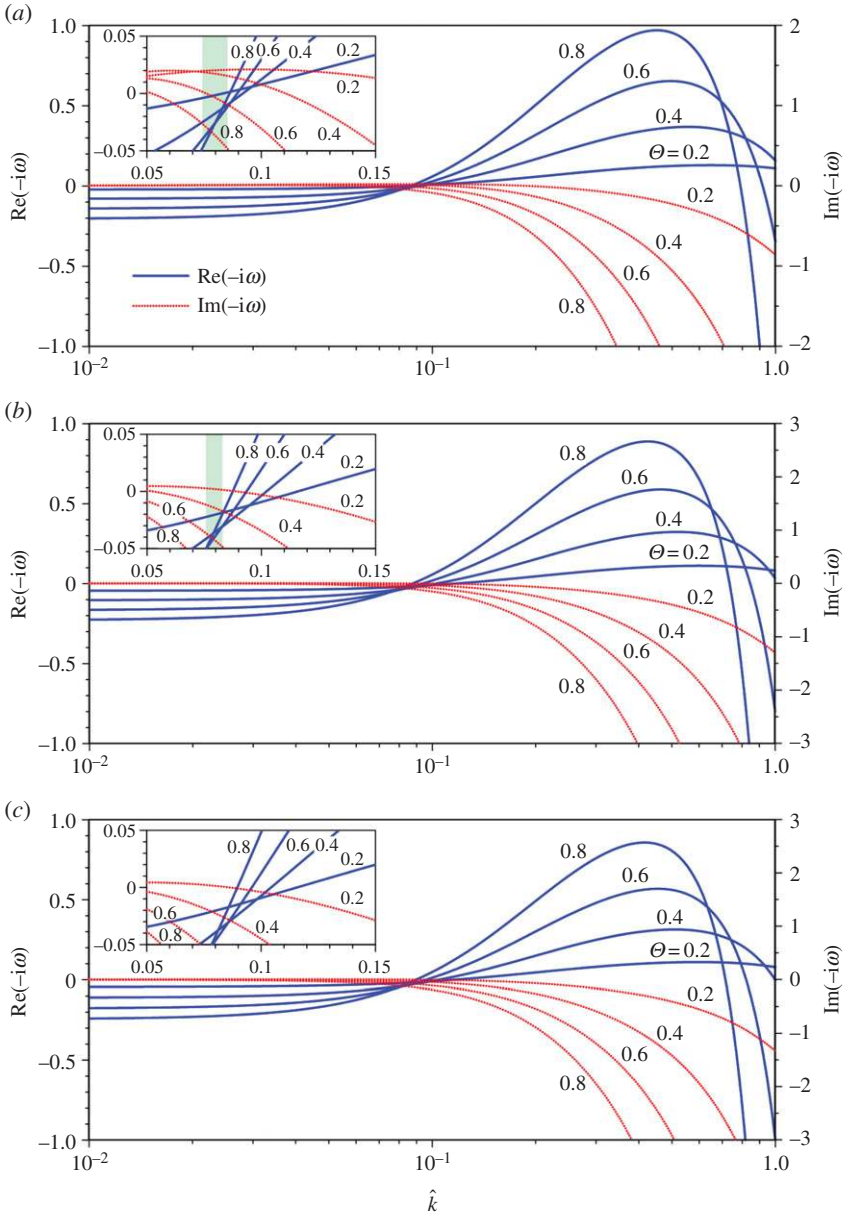

Figure 2. Variations of Re(−iω) and Im(−iω) with non-dimensional wavenumber $\hat{k}$ for aspect ratio $\mathcal{A} = 30$, relative roughness number $\zeta = 0.005$, Shields number $\Theta = 0.2$, 0.4, 0.6 and 0.8, and shear Reynolds numbers (*a*) $\mathcal{R}_* = 4$, (*b*) $\mathcal{R}_* = 20$ and (*c*) $\mathcal{R}_* = 500$. (Online version in colour.)

designate the lower and upper bounds of a variable, respectively. The band of wavenumbers is shown by the faded vertical strips (see figure 2 and also figures 3 and 4). Such a band can be envisaged as the *onset wavenumber band* for which the natural perturbation modes neither grow nor decay, suggesting that the natural perturbation modes maintain an equilibrium state. Physically, this can be interpreted as follows: a straight river with an unperturbed bed is generally unstable when the large-scale bed perturbations grow over a broad spectrum of external flow variables. Under such circumstances, there exists a set of wavenumbers which try to maintain the straight course of a river at the limiting state, causing the onset of the meandering of a

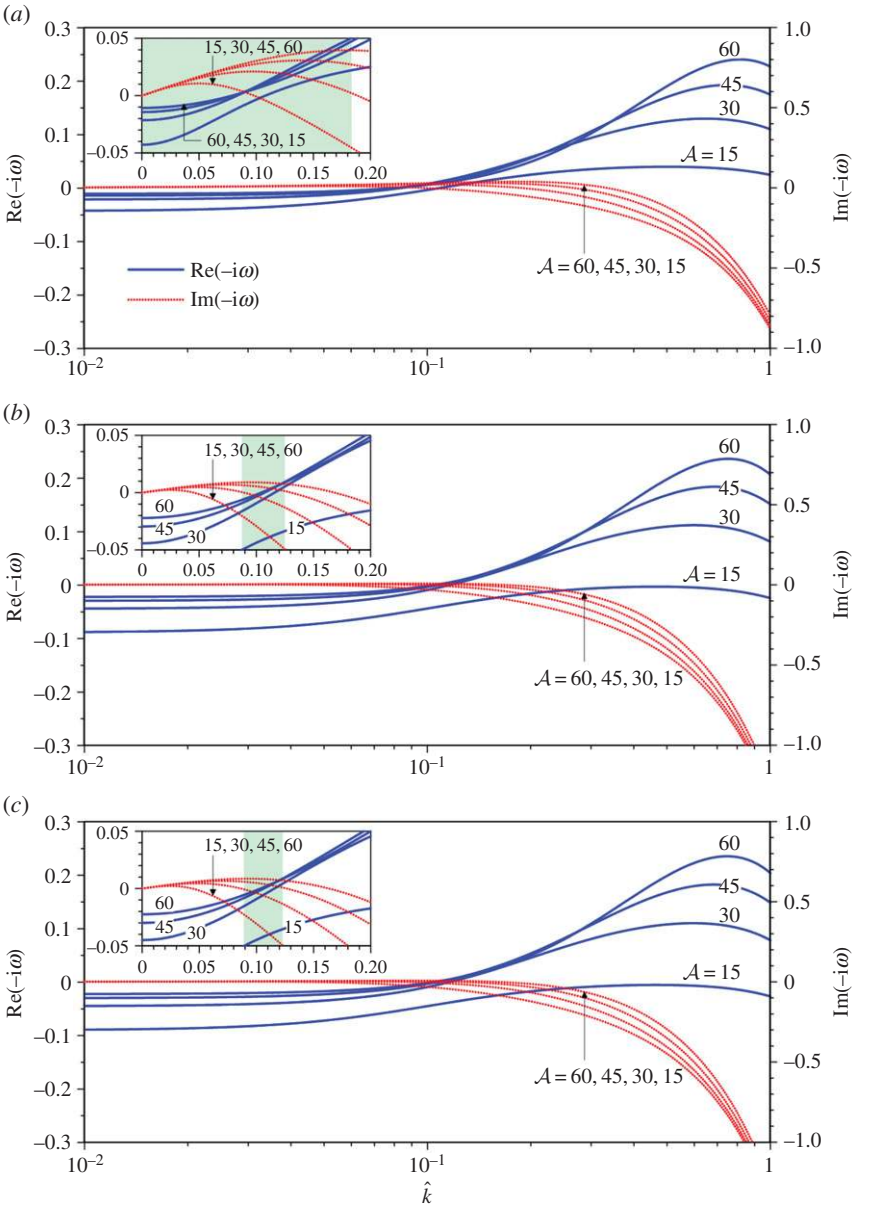

Figure 3. Variations of Re(−iω) and Im(−iω) with non-dimensional wavenumber $\hat{k}$ for aspect ratios $\mathcal{A} = 15, 30, 45$ and 60, relative roughness number $\zeta = 0.005$, Shields number $\Theta = 0.2$ and shear Reynolds numbers (*a*) $\mathcal{R}_* = 4$, (*b*) $\mathcal{R}_* = 20$ and (*c*) $\mathcal{R}_* = 500$. (Online version in colour.)

river. Reverting to figure 2, in the hydraulically smooth flow regime ($\mathcal{R}_* = 4$), the bandwidth is slightly larger than that in the hydraulically transitional flow regime ($\mathcal{R}_* = 20$). Surprisingly, for $\Theta \in [0.2, 0.8]$, no such band appears in the hydraulically rough flow regime ($\mathcal{R}_* = 500$). However, for $\mathcal{R}_* = 500$, the finite range of $\hat{k}_c$ is possible when the upper limit of the Shields number becomes less than 0.8 (say, $\Theta_u = 0.4$ and 0.6). It may be pointed out that the bandwidth increases when the difference between the Θ_u and Θ_l decreases, as apparent from the insets shown in figure 2*a*,*b*.

It is further interesting to study the evolutions of Re(−iω) and Im(−iω) for different aspect ratios $\mathcal{A}$ by keeping the relative roughness number ζ and the Shields number Θ constant. The variations of Re(−iω) and Im(−iω) with non-dimensional wavenumber $\hat{k}$ for $\mathcal{A} = 15$, 30, 45, 60,

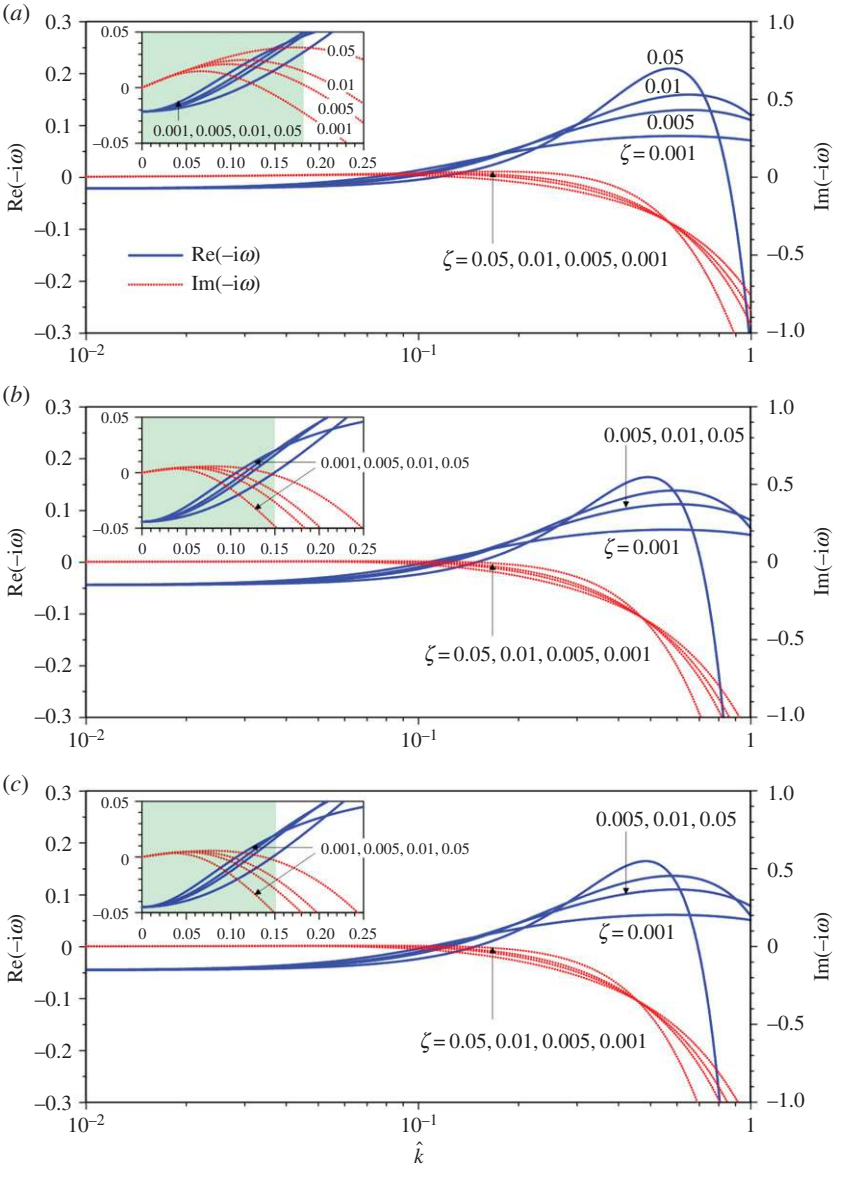

Figure 4. Variations of Re(−iω) and Im(−iω) with non-dimensional wavenumber $\hat{k}$ for aspect ratio $\mathcal{A} = 30$, relative roughness numbers $\zeta = 0.001$, 0.005, 0.01 and 0.05, Shields number $\Theta = 0.2$ and shear Reynolds numbers (*a*) $\mathcal{R}_* = 4$, (*b*) $\mathcal{R}_* = 20$ and (*c*) $\mathcal{R}_* = 500$. (Online version in colour.)

$\zeta = 0.005$, $\Theta = 0.2$, and $\mathcal{R}_* = 4$, 20 and 500 are illustrated in figure 3*a–c*. For a given $\mathcal{R}_*$ and $\hat{k}$ with $\hat{k} < 0.1$, the Re(−iω) decays with a decrease in $\mathcal{A}$. On the contrary, for a given $\hat{k}$ with $\hat{k} > 0.1$, the Re(−iω) grows with an increase in $\mathcal{A}$. From the variations of Im(−iω) with $\hat{k}$ for a specific flow regime, it is possible that, for a given $\hat{k}$ with $\hat{k} \ll 0.1$, the frequency of excitation is practically independent of $\mathcal{A}$. However, for a given $\hat{k}$ with $\hat{k} > 0.1$, the frequency of excitation rapidly decays with a decrease in $\mathcal{A}$ (figure 3*a–c*). Similar to figure 2, the onset wavenumber bands, which are furnished in the insets of figure 3, obey a generalized relationship of the form: $\hat{k}_c = \hat{k}\{[\text{Re}(-\text{i}\omega), \text{Im}(-\text{i}\omega)](\mathcal{A} = \mathcal{A}_1)\} \cap \hat{k}\{[\text{Re}(-\text{i}\omega), \text{Im}(-\text{i}\omega)](\mathcal{A} = \mathcal{A}_2)\} \ldots$ subject to the conditions: $[\text{Re}(-\text{i}\omega), \text{Im}(-\text{i}\omega)] \in [-0.05, 0.05]$ and $(\mathcal{A}_1, \mathcal{A}_2, \ldots) \in [\mathcal{A}_l, \mathcal{A}_u]$. In the hydraulically smooth flow regime ($\mathcal{R}_* = 4$), the bandwidth is larger than those in the hydraulically transitional ($\mathcal{R}_* = 20$) and rough ($\mathcal{R}_* = 500$) flow regimes.

Finally, we study the evolutions of Re($-$iω) and Im($-$iω) for different relative roughness numbers ζ by keeping the aspect ratio $\mathcal{A}$ and the Shields number Θ constant. Figure 4*a–c* demonstrates the variations of Re($-$iω) and Im($-$iω) with non-dimensional wavenumber $\hat{k}$ for $\mathcal{A}=30$, $\zeta=0.001$, 0.005, 0.01, 0.05, $\Theta=0.2$, and $\mathcal{R}_*=4$, 20 and 500. For a given $\mathcal{R}_*$ and $\hat{k}$ with $\hat{k}<0.1$, the Re($-$iω) reduces with an increase in ζ. On the contrary, for a given $\hat{k}$ with $\hat{k}>0.1$, there is no particular sequence in the variation of Re($-$iω) with ζ. The variations of Im($-$iω) with $\hat{k}$ for a specific flow regime elucidate that, for a given $\hat{k}$ with $\hat{k}\ll 0.1$, the frequency of excitation is invariant of ζ. Furthermore, for a given $\hat{k}\in(0.1,0.5)$, the frequency of excitation gently dampens with a decrease in ζ. By contrast, for a given $\hat{k}\in(0.5,1)$, the frequency of excitation dampens with ζ (figure 4*a–c*). In the insets of figure 4, the onset wavenumber bands are also shown. They correspond to a generalized form: $\hat{k}_c=\hat{k}\{[\mathrm{Re}(-\mathrm{i}\omega),\ \mathrm{Im}(-\mathrm{i}\omega)](\zeta=\zeta_1)\}\cap\hat{k}\{[\mathrm{Re}(-\mathrm{i}\omega),\ \mathrm{Im}(-\mathrm{i}\omega)](\zeta=\zeta_2)\}\ldots$ subject to the conditions: $[\mathrm{Re}(-\mathrm{i}\omega),\ \mathrm{Im}(-\mathrm{i}\omega)]\in[-0.05,0.05]$ and $(\zeta_1,\zeta_2,\ldots)\in[\zeta_l,\zeta_u]$. It is discernible that in the hydraulically smooth flow regime ($\mathcal{R}_*=4$) the bandwidth is somewhat larger than those in the hydraulically transitional ($\mathcal{R}_*=20$) and rough ($\mathcal{R}_*=500$) flow regimes.

So far, from the stability analysis, it is clearly understood how the natural river responds to external perturbations by elucidating the existence of typical onset wavenumber bands over a wide range of key variables. However, this analysis has not given any evidence for how the external instability evolves into the onset of meandering of a straight river from the phenomenological viewpoint. To progress further and gain an insight into this phenomenological mechanism, we present a phenomenological framework of the onset of the meandering a river in the following section. Then, this framework is further enlightened by presenting a theorem (universal scaling law) originating from the phenomenology of a turbulent energy cascade to offer a quantitative insight into the onset criterion.

3. Phenomenological framework of the onset of the meandering of a straight river

(a) Theoretical description

Let us start again with a straight river (figure 5*a*,*b*) with a width $2\mathcal{B}$, an unperturbed flow depth $\mathcal{D}_m$ and a longitudinal riverbed slope S, and carrying a steady flow discharge Q. The river flows turbulently with an average flow velocity $\mathcal{U}_m$ over a rough sediment bed, having a median size d of sediment grains. The turbulent flow structures can be organized in two ways [38]: (i) the macro-turbulent eddies, E_1, E_2 etc., having a velocity scale U_L, are primarily responsible for the erosion and deposition of sediment grains from the riverbed (figure 5*a*) and (ii) the micro-turbulent eddies, e_1, having a velocity scale u_l (resolved into u_n and u_t components), play a major role in transferring the flow momentum by straddling the wetted surface at the summit of the sediment grains (figure 5*b*).

In fact, the macro-turbulent eddies can evolve in both smooth and rough mobile beds, regardless of the bed formation. The length scale L of such eddies is proportional to the external geometric dimension of a river (say, flow depth $\mathcal{D}_m$), and their velocity scale U_L is proportional to the mean flow velocity $\mathcal{U}_m$ in a river [38]. On the other hand, the micro-turbulent eddies are characterized by the length scale l of the order of the sediment grain size d. Then, how does the process of meandering start in a straight river? The turbulent structure in the close proximity of the riverbed is essentially anisotropic in nature, implying that the fluctuations of turbulent velocity components have directional preference [39]. This anisotropy leads to the formation of turbulence-induced secondary currents, called *the secondary currents of Prandtl's second kind* [39,40]. It is however pertinent to emphasize that the secondary currents of Prandtl's second kind are suppressed by the helicoidal flow induced by the curvilinear flow streamlines in a developed meandering course, called *the secondary currents of Prandtl's first kind* [39]. Here, we consider the onset of the meandering of a straight river rather than a developed meandering course. Therefore, reverting to the straight river case as shown in figure 5, the macro-turbulent eddy

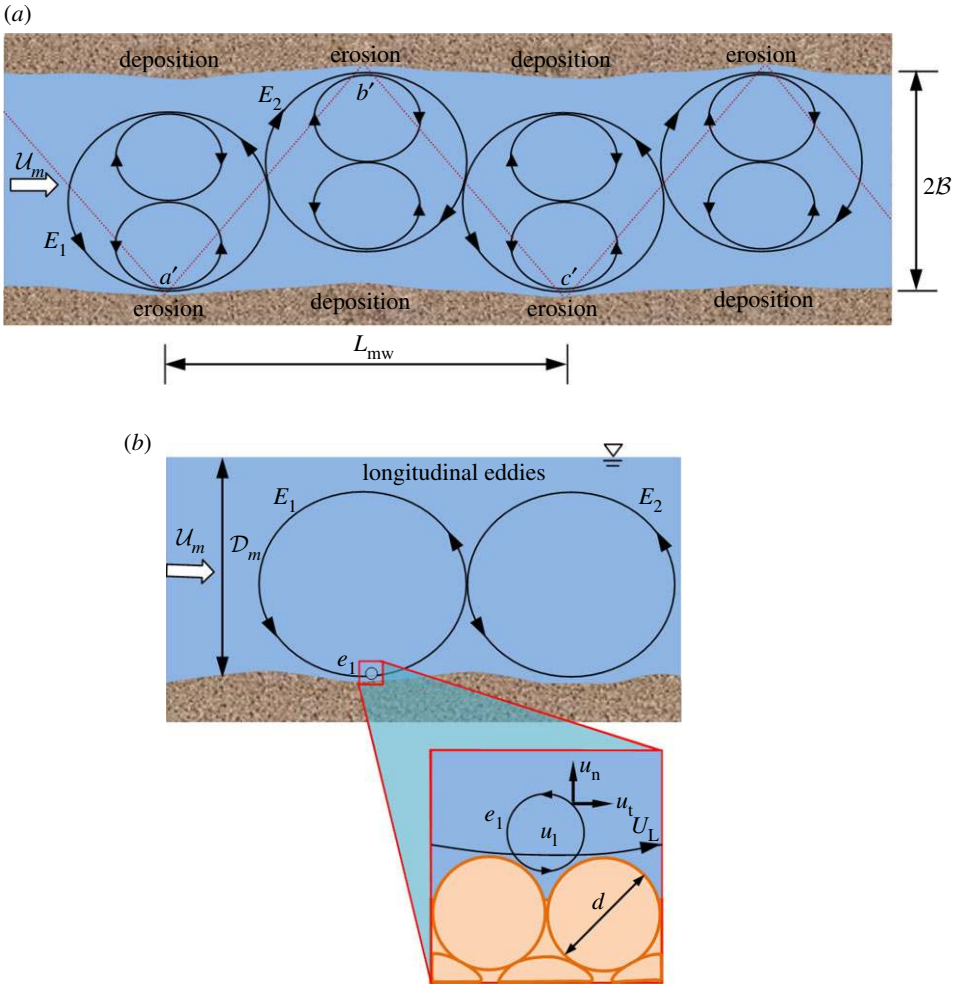

Figure 5. Sketch of a straight river illustrating the onset of meandering. (*a*) Plan view and (*b*) longitudinal view. The dotted lines in the plan view represent the sequential traversing of a gravity wave between the alternate bars. The meandering wavelength is denoted by L_{mw}. At a given time duration, the distance $a'b'c'$ represents the total distance covered by the gravity wave between the alternate bars, and the distance $a'c'$ indicates the straight path covered by the mean river flow. (Online version in colour.)

E_1 (figure 5*a*), being spheroidal in nature due to the local anisotropy and inherent instability, tends to move arbitrarily towards one of the riverbanks (let us consider towards the right bank). This movement is highly intermittent in nature as the anisotropy stretches the localized eddy towards the preferential direction. This spanwise shifting of the macro-turbulent eddies was experimentally evidenced in turbulent flow over a rough bed [41]. As this eddy has a counter-clockwise rotation as illustrated in figure 5*a*, it starts eroding the local sediment grains close to the right bank. In essence, this eddy can be envisaged as a spheroidal fluid parcel, containing a counter-rotating eddy that governs the spatial acceleration and deceleration of the flow patterns. The eroded sediment grains are subsequently deposited on the opposite side of the bank (figure 5*a*). Subsequently, an important question arises: is eddy E_1 stable? In fact, the experimental observations evidenced that the macro-turbulent eddies over a rough bed (as considered in this study) are relatively stable compared with those over a smooth bed [39]. We then pay attention to the adjacent localized eddy E_2, which is powered by the motion of eddy E_1, and therefore eddy E_2 is characterized by a clockwise rotation with an affinity to shift towards

the left bank. As a result of this, the eroded sediment grains from the left bank are deposited on the opposite side. In this way, the processes of alternate erosion and deposition advance as we proceed in the flow direction. This phenomenon of the motion of eddies is analogous to the motion of successive adjoining solid spheres (making a row) confined to two guided boundaries. When a counter-clockwise rotation is set to the first sphere with a slight shift towards the right boundary, then the next adjacent sphere has an opposite sense of rotation with an identical shift towards the left boundary. For the other spheres, a similar alternate process of rotation and shift occurs, as if the line joining the centres of the spheres forms a zigzag course. Therefore, the processes of alternate erosion and deposition of sediment grains in the riverbed by the action of macro-turbulent eddies are comprehended from this simple physical mechanism. Importantly, the emergence of such successive eddies generates gravity waves with a speed $\mathcal{U}_w$ proportional to $(g\mathcal{D}_m)^{0.5}$ [42,43]. The waves sequentially traverse the riverbank (indicated by the dotted lines in figure 5*a*), leaving a generic signature of the meandering wavelength L_{mw} [17,42,43]. This precisely explains the underlying mechanism of the onset of the meandering of a straight river.

Subsequently the question arises: how can we specifically set a quantitative onset criterion or a straight river to meander? To this end, we apply the concept of equal periodicity [42], stating that the time taken by the gravity wave to move across the distance between the alternate bars is equal to the time taken by the mean flow in a river to reach the straight path between the alternate bars. The mean flow velocity principally depends on the sediment grain size and has a link with the laws of a turbulent spectrum [38]. We apply the phenomenology of a turbulent energy cascade [28] to obtain a universal scaling law among the longitudinal riverbed slope, river width, flow discharge and median grain size.

Theorem 3.1. *At the onset of the meandering of a straight river, the longitudinal riverbed slope obeys the '2/9', '–2/9', '1/3' and '1/9' scaling laws with the river half-width, the flow discharge, the median grain size and the gravitational acceleration, respectively.*

Proof. The kinetic energy per unit mass of a turbulent eddy, characterized by the velocity scale u_l and the length scale l, is given by [28,38]

$$u_l^2 \propto \int_{1/l}^{\infty} E(k_w)\,\mathrm{d}k_w, \tag{3.1}$$

where $E(k_w)$ denotes the turbulent energy spectrum function and k_w denotes the wavenumber ($\propto 1/l$). The $E(k_w)$ can be expressed as $E(k_w) \propto U_L^2 L^{1+\sigma} k_w^{\sigma}$ [38], where U_L is the velocity scale of the macro-turbulent eddies, having the length scale L, with σ the spectral exponent. Substituting this expression for $E(k_w)$ into equation (3.1), the link between the microscopic and macroscopic velocity scales is obtained as

$$u_l \propto U_L \left(\frac{l}{L}\right)^{-(1+\sigma)/2}. \tag{3.2}$$

In close proximity to the bed sediment grains, a localized turbulent eddy interacts with the grains, giving rise to fluid-induced shear stress at the surface tangential to the summit of the sediment grains forming the riverbed (figure 5*b*). The velocity u_l of this localized turbulent eddy can be split into two components. They are the tangential velocity component u_t and the normal velocity component u_n. When the eddy size is of the order of a sediment grain size ($l \propto d$) such that it completely triggers the interspace between the two neighbouring sediment grains, then we can write $u_t \propto \mathcal{U}_m$ and $u_n \propto u_l$ [38]. Therefore, the fluid shear stress τ_f at the riverbed becomes $\tau_f = \rho_f \overline{u_t u_n}$, where the overbar indicates the time averaging over turbulence. Using equation (3.2) and noting that $(U_L, L) \propto (\mathcal{U}_m, \mathcal{D}_m)$, we get $\tau_f \propto \mathcal{U}_m^2 (d/\mathcal{D}_m)^{-(1+\sigma)/2}$. By contrast, the gravitational stress generated at the riverbed is expressed as $\tau_g = \rho_f g \mathcal{D}_m S$ [18]. Equating $\tau_f = \tau_g$, we obtain

$$\mathcal{U}_m = a_1 (g\mathcal{D}_m S)^{1/2} \left(\frac{d}{\mathcal{D}_m}\right)^{(1+\sigma)/4}, \tag{3.3}$$

where a_1 is a coefficient.

The time taken by the river flow to cover the straight path between the alternate bars is $L_{\mathrm{mw}}/\mathcal{U}_m$, while the time period of the wave to cover this distance is $(L_{\mathrm{mw}}^2 + 16\mathcal{B}^2)^{1/2}/\mathcal{U}_{\mathrm{w}}$. The $\mathcal{U}_{\mathrm{w}}$ is given by $\mathcal{U}_{\mathrm{w}} = a_2(g\mathcal{D}_m)^{0.5}$ [42,43], where a_2 is a coefficient. Equating these time periods, we obtain

$$L_{\mathrm{mw}} = 4\mathcal{B}\left(\frac{\mathcal{U}_{\mathrm{w}}^2}{\mathcal{U}_m^2} - 1\right)^{-1/2}. \tag{3.4}$$

For a real solution of equation (3.4), we must have $\mathcal{U}_{\mathrm{w}} > \mathcal{U}_m$. Therefore, inserting the expressions for $\mathcal{U}_m$ and $\mathcal{U}_{\mathrm{w}}$ into the above inequality yields

$$\frac{a_2}{a_1} > S^{1/2}\left(\frac{d}{\mathcal{D}_m}\right)^{(1+\sigma)/4}. \tag{3.5}$$

The flow discharge is expressed as

$$Q = 2\mathcal{B}\mathcal{D}_m\mathcal{U}_m = 2a_1\mathcal{B}\mathcal{D}_m(g\mathcal{D}_m S)^{1/2}\left(\frac{d}{\mathcal{D}_m}\right)^{(1+\sigma)/4}. \tag{3.6}$$

Eliminating $\mathcal{D}_m$ from equations (3.5) and (3.6) results in the following scaling relationship: $S \propto \mathcal{B}^{-(1+\sigma)/3}Q^{(1+\sigma)/3}d^{-(1+\sigma)/2}g^{-(1+\sigma)/6}$. For a fully developed three-dimensional turbulence, we can write $\sigma = -\frac{1}{6}$ [28]. Thus, the desired scaling law is

$$S \propto \mathcal{B}^{2/9}Q^{-2/9}d^{1/3}g^{1/9}. \tag{3.7}$$

Note that the role of g in the right-hand side of equation (3.7) is to introduce the universality in the scaling law applicable not only to this planet but also to other planets. ■

(b) Results and discussion

Equation (3.7) provides a universal scaling law of the onset of the meandering of a straight river, elucidating the mechanism of the onset criterion. This relationship is dimensionally homogeneous and brings together all the necessary parameters of a river. It is worth noting that the phenomenological scaling law (see equation (3.7)) cannot explicitly anticipate the proportionality constant. Hence, the proportionality constant can only be obtained using the measured data of all the parameters. It is obvious that, for a constant value of the gravitational acceleration, the onset slope is proportional to the '−2/9'th power of the flow discharge for rivers, having nearly equal river width and sediment grain size. Figure 6 depicts the data plots of the longitudinal riverbed slope versus flow discharge measured in ample natural and model rivers [19,44], characterized by nearly straight to well-formed meanders. The average slope of the plotted data band shown by the straight line follows a '−2/9' scaling law. The overall scatter of the data is due to the variability of river widths and sediment grain sizes. It is now required to validate the present scaling law with the previously reported empirical formulae for the onset of the meandering of a straight river. We recall Lane's scaling: $S = 7 \times 10^{-4}Q^{-0.25}$ [19], whereas Ackers and Charlton's scaling reads: $S = 21 \times 10^{-4}Q^{-0.12}$ [45]. It may be noted that these empirical formulae were later verified by the experimental data of Schumm & Khan [46], who conducted a series of experiments to find the effects of longitudinal slope and sediment flux on river patterns. Therefore, the '−2/9' (= −0.22) law obtained from this study closely corresponds to that previously reported by Lane [19], whereas it slightly deviates from that obtained by Ackers & Charlton [45]. Furthermore, in the inset of figure 6, the dependency of the computed longitudinal riverbed slope S on $\mathcal{B}^{2/9}Q^{-2/9}d^{1/3}g^{1/9}$, as obtained from equation (3.7), is shown overlapping the data plots for some rivers, whose width, flow discharge and median grain size are available in the literature. These data plots are in agreement with the computed line for a value of the proportionality constant of 0.005, which should be a universal constant because equation (3.7) is a universal scaling law.

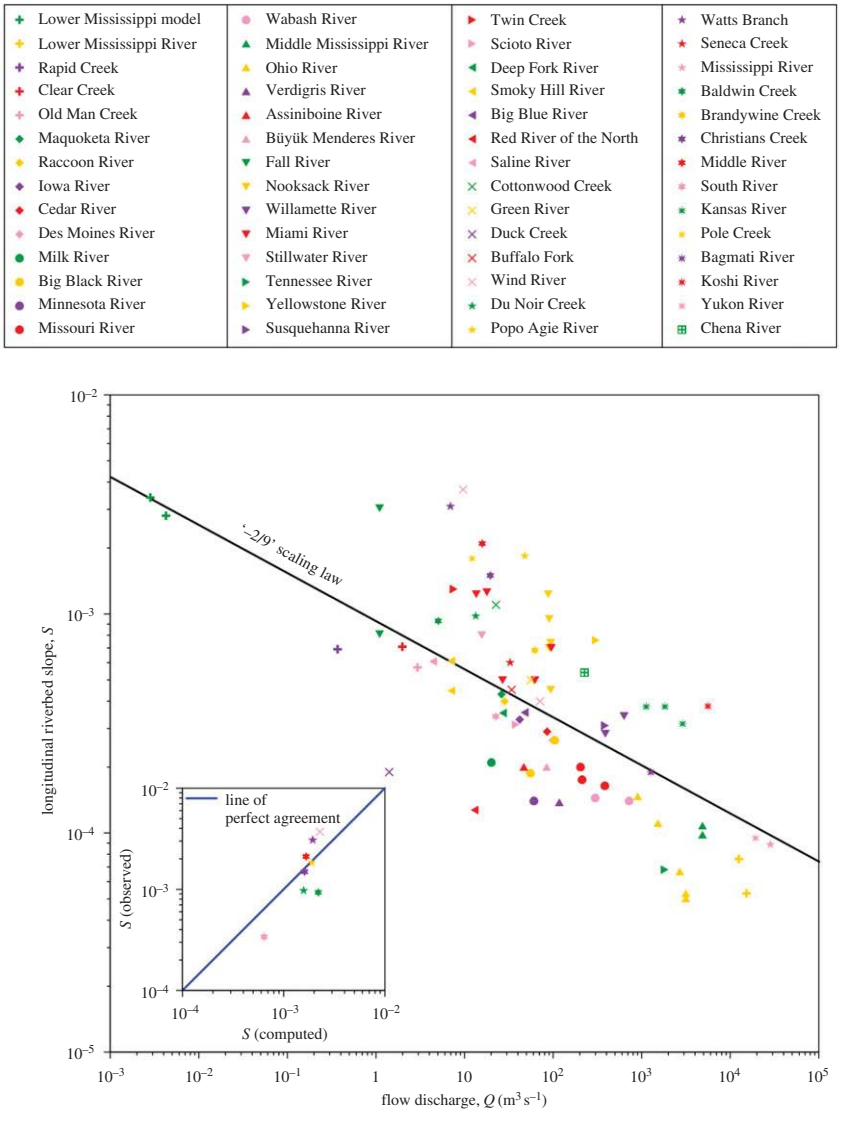

Figure 6. Longitudinal riverbed slope versus flow discharge relationship. The inset shows the dependency of the computed riverbed slope S on $\mathcal{B}^{2/9}Q^{-2/9}d^{1/3}g^{1/9}$ as obtained from equation (3.7), fitting the data plots for some rivers, whose width, flow discharge and median grain size are available in the literature. The measured data are taken from different rivers [19,44]. (Online version in colour.)

4. Conclusion

The origin of the onset of the meandering of a straight river is explored. By performing a stability analysis of a straight river, it has been established that there exists an onset wavenumber band for a specific flow regime for which the natural perturbation modes neither grow nor decay over a wide spectrum of aspect ratios, relative roughness numbers and Shields numbers. The genesis of the onset of the meandering of a river lies in the governing mechanism of a turbulent flow having a counter-rotation of the adjoining macro-turbulent eddies in succession to sustain the processes of alternate erosion and deposition of sediment grains. This concept, aided by the phenomenology of a turbulent energy cascade, has been able to discover the missing link between the longitudinal riverbed slope, river width, flow discharge, median grain size and gravitational acceleration by

establishing a theorem (universal scaling law) of the onset of the meandering of a straight river. The proposed universal scaling law preserves the dimensional homogeneity and corroborates the data obtained from the measurements in natural and model rivers. This study thus facilitates a general framework to achieve the true origin of the onset criterion for a river to meander.

Data accessibility. The data used in this study can be accessed from the following links: http://acwc.sdp.sirsi.net/client/en_US/search/asset/1045406;jsessionid=F8EF7D7E0332444DE708A3A3621505B7.enterprise-15000; https://www.uvm.edu/~wbowden/Teaching/Stream_Geomorph_Assess/Resources/Private/Documents/1957_leopold_wolman_channel_patterns.pdf.

Authors' contributions. The authors of this paper contributed jointly.

Competing interests. The authors declare that they have no competing interests.

Funding. No funding has been received for this article.

References

1. Vita-Finzi C. 2012 River history. *Phil. Trans. R. Soc. A* **370**, 2029–2039. (doi:10.1098/rsta.2011.0604)
2. Coulthard TJ, van De Wiel MJ. 2012 Modelling river history and evolution. *Phil. Trans. R. Soc. A* **370**, 2123–2142. (doi:10.1098/rsta.2011.0597)
3. Baker VR, Hamilton CW, Burr DM, Gulick VC, Komatsu G, Luo W, Rice Jr JW, Rodriguez JAP. 2015 Fluvial geomorphology on earth-like planetary surfaces: a review. *Geomorphology* **245**, 149–182. (doi:10.1016/j.geomorph.2015.05.002)
4. Choné G, Biron PM. 2016 Assessing the relationship between river mobility and habitat. *River Res. Applic.* **32**, 528–539. (doi:10.1002/rra.2896)
5. Gyr A. 2010 The meander paradox—a topological view. *Appl. Mech. Rev.* **63**, 020801. (doi:10.1115/1.4000725)
6. Hey RD. 1976 Geometry of river meanders. *Nature* **262**, 482–484. (doi:10.1038/262482a0)
7. Baker VR. 2013 Sinuous rivers. *Proc. Natl Acad. Sci. USA* **110**, 8321–8322. (doi:10.1073/pnas.1306619110)
8. Stølum HH. 1996 River meandering as a self-organization process. *Science* **271**, 1710–1713. (doi:10.1126/science.271.5256.1710)
9. Eakin HM. 1910 The influence of the earth's rotation upon the lateral erosion of streams. *J. Geol.* **18**, 435–447. (doi:org/10.1086/621757)
10. Einstein A. 1926 The cause of the formation of meanders in the courses of rivers and of the so called Baer's law. *Naturwissenschaften* **14**, 1–3.
11. Friedkin JF. 1945 *Laboratory study of the meandering of alluvial rivers*. Vicksburg, MS: United States Waterways Experiment Station.
12. Henderson FM. 1963 Stability of alluvial channels. *Trans. Am. Soc. Civ. Eng.* **128**, 657–686.
13. Tanner WF. 1960 Helicoidal flow, a possible cause of meandering. *J. Geophys. Res.* **65**, 993–995. (doi:10.1029/JZ065i003p00993)
14. Onishi Y, Jain SC, Kennedy JF. 1976 Effects of meandering in alluvial streams. *J. Hydraul. Div.* **112**, 899–917.
15. Yang CT. 1971 On river meanders. *J. Hydrol.* **13**, 231–253. (doi:10.1016/0022-1694(71)90226-5)
16. Yalin MS. 1977 *Mechanics of sediment transport*. Oxford, UK: Pergamon.
17. Einstein HA, Shen HW. 1964 A study on meandering in straight alluvial channels. *J. Geophys. Res.* **69**, 5239–5247. (doi:10.1029/JZ069i024p05239)
18. Dey S. 2014 *Fluvial hydrodynamics: hydrodynamic and sediment transport phenomena*. Berlin, Germany: Springer.
19. Lane EW. 1957 *A study of the shape of channels formed by natural streams flowing in erodible material*. Omaha, NE: United States Army Engineer Division, Missouri River Division, Corps of Engineers.
20. von Schelling H. 1951 Most frequent particle paths in a plane. *Trans. Am. Geophys. Union* **32**, 222–226. (doi:10.1029/TR032i002p00222)
21. Langbein WB, Leopold LB. 1966 River meanders—theory of minimum variance. Professional paper 422-H, United States Geological Survey, Washington, DC, pp. H1–H15.
22. Mecklenburg DE, Jayakaran AD. 2012 Dimensioning the sine-generated curve meander geometry. *J. Am. Water Resour. Assoc.* **48**, 635–642. (doi:10.1111/j.1752-1688.2012.00638.x)

23. Movshovitz-Hadar N, Shmukler A. 2006 The mathematics of river meanders. English translation of a paper in *Aleh, the Israel High School Math Teacher Journal*, 1998, no. 25, pp. 62–76. [In Hebrew.]
24. Callander RA. 1969 Instability and river channels. *J. Fluid Mech.* **36**, 465–480. (doi:10.1017/S0022112069001765)
25. Engelund F, Skovgaard O. 1973 On the origin of meandering and braiding in alluvial streams. *J. Fluid Mech.* **57**, 289–302. (doi:10.1017/S0022112073001163)
26. Fredsøe J. 1978 Meandering and braiding of rivers. *J. Fluid Mech.* **84**, 609–624. (doi:10.1017/S0022112078000373)
27. Blondeaux P, Seminara G. 1985 A unified bar-bend theory of river meanders. *J. Fluid Mech.* **157**, 449–470. (doi:10.1017/S0022112085002440)
28. Frisch U. 1995 *Turbulence: the legacy of A. N. Kolmogorov*. Cambridge, UK: Cambridge University Press.
29. de Saint-Venant B. 1871 Theorie du mouvement non permanent des eaux, avec application aux crues de rivieras et a l'introduction des marces dans leur lit. *C. R. Acad. Sci.* **73**, 147–154, 237–240.
30. Exner FM. 1925 Über die Wechselwirkung zwischen Wasser und Geschiebe in Flüssen. *Sitzungsberichte der Akademie der Wissenschaften* **134**, 165–203.
31. Colebrook CF, White CM. 1937 Experiments with fluid friction in roughened pipes. *Proc. R. Soc. Lond. A* **161**, 367–381. (doi:10.1098/rspa.1937.0150)
32. Engelund F, Hansen E. 1966 Investigations of flow in alluvial streams. *Acta Polytech. Scand.* **35**, 1–100.
33. Einstein HA. 1950 The bed-load function for sediment transportation in open channel flows. Technical bulletin 1026, United States Department of Agriculture, Soil Conservation Service, Washington, DC, USA.
34. Ikeda S. 1982 Lateral bed load transport on side slopes. *J. Hydraul. Div.* **108**, 1097–1099.
35. Talmon AM, Struiksma N, van Mierlo MCLM. 1995 Laboratory measurements of the direction of sediment transport on transverse alluvial-bed slopes. *J. Hydraul. Res.* **33**, 495–517. (doi:10.1080/00221689509498657)
36. Ali SZ, Dey S. 2016 Hydrodynamics of sediment threshold. *Phys. Fluids* **28**, 075103. (doi:10.1063/1.4955103)
37. Cao Z, Pender G, Meng J. 2006 Explicit formulation of the Shields diagram for incipient motion of sediment. *J. Hydraul. Eng.* **132**, 1097–1099. (doi:10.1061/(ASCE)0733-9429(2006)132:10(1097))
38. Ali SZ, Dey S. 2017 Origin of the scaling laws of sediment transport. *Proc. R. Soc. A* **473**, 20160785. (doi:10.1098/rspa.2016.0785)
39. Nezu I, Nakagawa H. 1993 *Turbulence in open-channel flows*. Rotterdam, The Netherlands: Balkema.
40. Einstein HA, Li H. 1958 Secondary currents in straight channels. *Trans. Am. Geophys. Union* **39**, 1085–1088. (doi:10.1029/TR039i006p01085)
41. Albayrak I, Lemmin U. 2011 Secondary currents and corresponding surface velocity patterns in a turbulent open-channel flow over a rough bed. *J. Hydraul. Eng.* **137**, 1318–1334. (doi:10.1061/(ASCE)HY.1943-7900.0000438)
42. Werner PW. 1951 On the origin of river meanders. *Trans. Am. Geophys. Union* **32**, 898–902. (doi:10.1029/TR032i006p00898)
43. Eaton BC, Church M, Davies TRH. 2006 A conceptual model for meander initiation in bedload-dominated streams. *Earth Surf. Process. Landf.* **31**, 875–891. (doi:10.1002/esp.1297)
44. Leopold LB, Wolman MG. 1957 River channel patterns: braided, meandering and straight. Professional paper 282-B, United States Geological Survey, Washington, DC, USA.
45. Ackers P, Charlton FG. 1970 Summary of paper 7362. The slope and resistance of small meandering channels. *Proc. Inst. Civ. Eng.* **47**, 388. (doi:10.1680/iicep.1970.6579)
46. Schumm SA, Khan HR. 1972 Experimental study of channel patterns. *Geol. Soc. Am. Bull.* **83**, 1755–1770. (doi:10.1130/0016-7606(1972)83[1755:ESOCP]2.0.CO;2)